Accelerated carbonation of brucite in mine tailings for carbon sequestration

Journal:	*Environmental Science & Technology*
Manuscript ID:	es-2012-012854.R2
Manuscript Type:	Article
Date Submitted by the Author:	02-Jul-2012
Complete List of Authors:	Harrison, Anna; University of British Columbia, Earth and Ocean Sciences Power, Ian; University of British Columbia, Earth and Ocean Sciences Dipple, Gregory; University of British Columbia, Earth and Ocean Sciences

Accelerated carbonation of brucite in mine tailings for carbon sequestration

Anna L. Harrison*, Ian M. Power, and Gregory M. Dipple

Mineral Deposit Research Unit, Department of Earth and Ocean Sciences, The University of British Columbia, 6339 Stores Road, Vancouver, British Columbia V6T 1Z4, Canada.

ALH* – aharriso@eos.ubc.ca; IMP – ipower@eos.ubc.ca; GMD – gdipple@eos.ubc.ca.

*Corresponding author (phone: 1 778 990 4325; fax: 1 604 822 6088; email: aharriso@eos.ubc.ca).

Abstract

Atmospheric CO_2 is sequestered within ultramafic mine tailings via carbonation of Mg-bearing minerals. The rate of carbon sequestration at some mine sites appears to be limited by the rate of CO_2 supply. If carbonation of bulk tailings were accelerated, large mines may have the capacity to sequester millions of tonnes of CO_2 annually, offsetting mine emissions. The effect of supplying elevated partial pressures of CO_2 (pCO_2) at 1 atm total pressure, on the carbonation rate of brucite [$Mg(OH)_2$], a tailings mineral, was investigated experimentally with conditions emulating those at Mount Keith Nickel Mine (MKM), Western Australia. Brucite was carbonated to form nesquehonite [$MgCO_3 \cdot 3H_2O$] at a rate that increased linearly with pCO_2. Geochemical modeling indicated that HCO_3^- promoted dissolution accelerated brucite carbonation. Isotopic and aqueous chemistry data indicated that equilibrium between CO_2 in the gas and aqueous phases was not attained during carbonation, yet nesquehonite precipitation occurred at equilibrium. This implies CO_2 uptake into solution remains rate-limiting for brucite carbonation at elevated pCO_2, providing potential for further acceleration. Accelerated brucite carbonation at MKM offers the potential to offset annual mine emissions by ~22-57%. Recognition of mechanisms for brucite carbonation will guide ongoing work to accelerate Mg-silicate carbonation in tailings.

Introduction

The accumulation of anthropogenic greenhouse gases (GHGs), predominantly CO_2, in the atmosphere has been identified as a cause of climate change.[1] Carbon sequestration is one of many strategies necessary to stabilize CO_2 concentrations while transitioning to alternative energy sources.[2-5] Carbon mineralization involves dissolution of non-carbonate minerals (e.g., silicates, hydroxides, and oxides) and subsequent precipitation of carbonate minerals, which sequesters CO_2.[5-8] This is a promising option for carbon sequestration as carbonate minerals are environmentally benign and stable, providing little possibility of accidental release and reducing the need for post-storage monitoring.[7,9] Research in carbon mineralization has largely focused on industrial processes that use elevated temperatures and pressures to accelerate carbonation reaction rates (e.g., 185°C, 150 atm),[9-15] however, the financial and energy costs of such methods limits their viability. To avoid such costs, research has been directed towards developing carbon mineralization strategies at low temperature and pressure conditions.[16-22] Carbonation of industrial wastes such as steel and blast furnace slag, and alkaline and saline waste water is advantageous as it exploits available waste materials.[23-35]

Passive carbon mineralization in mine tailings under normal mining conditions has been well documented.[18,21,24,30,36] This process has been recognized at historic and active Canadian chrysotile and diamond mines,[18,21,24] and at the active Mount Keith Nickel Mine (MKM) in Western Australia.[37] Carbonation of tailings is facilitated by high surface areas,[18] yet at MKM, reaction rates are limited by the uptake of CO_2 into solution.[30,38] If passive carbonation of bulk tailings were accelerated at large mines, it could more than offset the GHG emissions of mining operations. Supplying elevated

(above atmospheric) partial pressures of CO_2 (pCO_2) into tailings may accelerate carbonation both by enhancing mineral dissolution due to increased acidity[39-41] and promoting carbonate mineral precipitation due to elevated dissolved inorganic carbon (DIC) concentration.

Carbonation of brucite [$Mg(OH)_2$], a common but minor component of ultramafic mine tailings, offers significant sequestration potential. It has been documented at between 1-15 wt.% in chrysotile tailings, nickel tailings and deposits, and in chromite ore processing residue.[22,37,42] In Québec, Canada, there is an estimated 2 Gt of chrysotile mining residue,[43] some of which contains 1.8 wt.% brucite.[22] If these brucite contents are representative of the entire chrysotile stockpile, up to 27 Mt of CO_2 could be sequestered via brucite carbonation alone. At active mine sites, accelerated carbonation of brucite in tailings provides the potential to significantly offset the annual GHG emissions of mining operations. At MKM, ~11 Mt of tailings are produced annually, containing 0.11-0.28 Mt brucite.[37,44] Carbonation of the brucite produced annually would offset mine emissions (370 kt/year CO_2 equivalent)[44] by 22-57%. Yet, passive carbonation rates at MKM and the Black Lake chrysotile mine in Québec are estimated at only ~56[37] and ~0.6 kt/year,[36] respectively. Incorporation of accelerated carbonation methods in the design of prospective mines offers the potential to significantly offset emissions throughout the lifetime of mining operations. At the Dumont Nickel deposit in Québec, for instance, assuming homogeneous brucite distribution in processed nickel ore of 10-15 wt.%[22] and a similar scale of operations as MKM, accelerated brucite carbonation could exceed that predicted for MKM. Therefore, despite its minor abundance, brucite carbonation could provide a meaningful CO_2 sink on the scale of mine emissions.

The goal of this study was to investigate the mechanisms of brucite carbonation in mine tailings and to identify the rate-limiting steps in order to design methods for accelerating carbon sequestration in tailings. The effect of elevated pCO_2 at 1 atm total pressure on the carbonation rate of brucite was investigated experimentally in batch reactors. Investigation of brucite carbonation may also guide ongoing work to accelerate carbonation of Mg-silicate minerals in tailings, which constitute the majority of ultramafic tailings and offer greater total sequestration capacity.

Methods

Brucite slurries (3.0 L) were prepared in side arm flasks (SI Figure S1). The solution composition mimicked that of pore water at MKM (1.0 M NaCl, and 0.1 M $MgCl_2 \cdot 6H_2O$).[45] High purity pulverized brucite ore (150 g; grain size = 2-40 μm diameter; surface area = 6.6 m^2/g) from Brucite Mine, Nevada was added to each solution just prior to supplying CO_2 gas. Rietveld refinement of X-ray diffraction (XRD) data indicated the brucite ore was between 90-95 wt.% brucite with minor dolomite and trace lizardite. Mixtures of CO_2 and N_2 gas were bubbled into continuously stirred slurries using glass sparge tubes. Gases were blended using a two-tube gas blender. CO_2 concentration of the supplied gas stream was varied between experiments for values of 10%, 50%, and 100% CO_2 at a total flow rate of 540 mL/min, which was divided evenly between duplicate experiments that were run simultaneously. Duplicate experiments are henceforth referred to as 'X% CO_2 1 and 2.' Three experiments were run using laboratory air ($pCO_2 \approx 0.04\%$) supplied at ~270 mL/min using a peristaltic pump to act as experimental controls and establish the carbonation rate at low pCO_2. Slight differences

in the reactivity of duplicate reactors occurred due to imperfect mixing that resulted in occasional settling of brucite particles, which were re-suspended manually when observed.

Flasks were vented through the side arm to maintain atmospheric pressure. The exhaust of high pCO_2 experiments was directed into a Los Gatos Research (LGR)® off-axis integrated cavity output laser spectrometer for continuous measurement of CO_2 concentration.[46] All gas composition data represent the combined exhaust from duplicate, simultaneous, high pCO_2 reactors.

Slurry temperature and pH were measured routinely and water samples for DIC and Mg concentrations ([Mg]), and $\delta^{13}C_{DIC}$[47] were collected regularly. Solid samples were taken at the same time for mineralogical analysis using XRD, $\delta^{13}C$ and carbon abundance (%C) analysis, and imaging using scanning electron microscopy (SEM). System mass before and after sampling and the mass of each sample were measured. At the end of each experiment, slurries were filtered to collect and weigh all solids.

The experimental durations were 198, 56, and 72 h for the 10%, 50%, and 100% CO_2 experiments, respectively. Two short-term experiments using atmospheric CO_2 were run for 56 and 72 h to serve as experimental controls (i.e., systems with negligible carbonation). A third atmospheric CO_2 experiment was conducted for 2856 h to establish background carbonation rates. The high pCO_2 experiments were terminated upon achievement of steady-state conditions. For further details regarding experimental setup and analytical techniques, refer to the Supporting information (SI).

Results and Discussion

Chemical environment. There are three main requirements to allow carbonation to occur *in situ* in tailings facilities: (1) CO_2 is available in solution as DIC, (2) cations are available, and (3) the chemical environment promotes both tailings mineral dissolution (cation leaching), and carbonate mineral precipitation (Figure 1).

In all reactors, initial pH values following brucite addition were between 9.3 and 9.4 and initial DIC concentration ranged from 15 to 26 mg/L. Initial DIC content is attributed to dissolution of laboratory air into the saline solutions prior to sparging of gas. In the 10% and 50% CO_2 reactors, an abrupt initial drop in pH was followed by a period of relatively constant pH before declining to a final stable pH of ~7.6 and ~7.1 in the 10% and 50% experiments, respectively (Figure 2A). In the 100% CO_2 reactors pH declined rapidly to a minimum stable value of ~6.9 after 10 h. Initial drops in pH were coincident with rapid increases in both DIC and [Mg] in all high pCO_2 reactors owing to $CO_{2(g)}$ and brucite dissolution, respectively (Figures 2A, 3A-B). The pH value and duration of the first pH stabilization and final pH were dependent on the pCO_2 in the reactor atmospheres (Figure 2A). During the first 6-8 h in the 10% CO_2 experiments, DIC and [Mg] increased, before declining to reach near constant values during the period of 12-46 h (Figures 3A-B). The relatively stable DIC during this period is indicative of a quasi-steady-state wherein brucite carbonation was balanced by CO_2 uptake into solution. The final stable pH value was lower at higher pCO_2, resulting in a greater proportion of Mg and DIC remaining in solution (Figures 2A, 3A-B, Table 1). Final DIC and [Mg] stabilized approximately at equilibrium with the hydrated carbonate mineral, nesquehonite [$MgCO_3 \cdot 3H_2O$], as calculated with PHREEQC[48] using the Pitzer database (Figure 3A-B).

In the long-term atmospheric CO_2 experiment, pH reached a minimum of 9.0. An initial increase in DIC in this experiment to 80 mg/L after 192 h was followed by a decline to 33 mg/L after 2856 h (Figure 2B). This implies DIC was removed faster than it was replaced by uptake of $CO_{2(g)}$ into solution, with the converse true at early time. A 0.02 M increase in [Mg] in this experiment was consistent with evapoconcentration, with no significant change in [Mg] in the controls (SI Figure S2). This implies brucite dissolution was slow in the controls, and was balanced by the rate of Mg-carbonate precipitation in the long-term experiment.

In all high pCO_2 experiments, the decline in pH from alkaline to circumneutral conditions was driven by the uptake of CO_2. Although low pH accelerates brucite dissolution,[41] carbonate precipitation is generally favored at higher pH values.[27,49-51] As such, some mineral carbonation processes have been designed such that cation extraction and carbonate precipitation are achieved in separate steps.[9,49,50,52] *In situ* carbon mineralization in mine tailings requires these processes to occur concurrently. The chemical environment must promote tailings mineral dissolution yet permit carbonate precipitation. The high pCO_2 experiments indicated that both brucite dissolution and carbonate precipitation are promoted with elevated pCO_2 at atmospheric pressure and temperature, suggesting that accelerated *in situ* carbonation of brucite may be achieved in ultramafic tailings, provided the brucite content is sufficient.

CO_2 concentration in the exhaust gas from duplicate reactors in the 10% CO_2 and 50% CO_2 experiments was reduced by up to 45% and 44%, respectively at the onset of each experiment, implying carbonation began immediately (SI Figure S3). No change in gas composition was measurable in the 100% CO_2 experiment as the entire volume of gas

consisted of CO_2. In all high pCO_2 experiments, 43-51% of CO_2 supplied during the carbonation reaction was sequestered (Table 1).

Owing to the exothermic nature of the reaction, an increase in slurry temperature in high pCO_2 reactors over that of experimental controls was noted throughout carbonation, although the experiments were not insulated (SI Figure S4). Diurnal temperature variations in the laboratory resulted in periodic fluctuations in slurry temperature in all experiments (SI Figure S4). Control temperature was exceeded by a maximum of 5.4 ± 0.5°C. The enthalpy of reaction for brucite carbonation is -75.1 kJ/mol,[53] corresponding to a total of ~129 kJ of energy released in the 100% CO_2 experiments based on the average mass of nesquehonite formed, providing the potential to heat the 3.0 L of water by 10.3°C. This suggests heat was lost to the surroundings. Temperature may provide a useful indicator for reaction progress and be utilized to monitor and map carbonation in tailings facilities that contain sufficient brucite.[36]

Brucite dissolution and carbonation rates. The rates of brucite dissolution and carbonation were accelerated linearly with pCO_2, resulting in a ~2400-fold increase in carbonation rate with an increase from atmospheric pCO_2 (~0.04%) to 100% CO_2 (Figure 4). Both dissolution and carbonation rates were calculated as averages over the entire reaction, making comparison with published dissolution rates difficult, as the instantaneous rate of reaction may change with time. Brucite dissolution was calculated as follows (eq. 1):

$$\text{Rate} = m_{ibrc} / (SA_{ibrc} \times t_c) \qquad \text{(eq. 1)}$$

Where m_{ibrc} is the initial moles of brucite, SA_{ibrc} is the total initial brucite surface area (m^2), and t_c is the time for complete carbonation (s) as estimated with XRD, %C, and pH data (Figure 2A, SI Figures S5-S6). Reaction end times of 75 h for 10% CO_2 1 and 2, 14 and 12 h for 50% CO_2 1 and 2, respectively, and 7 h were estimated for both 100% CO_2 experiments. Average dissolution rates in duplicate reactors were 9.7×10^{-9}, 5.6×10^{-8} and 1.0×10^{-7} mol/m^2/s with 10%, 50%, and 100% CO_2, respectively. The brucite dissolution rates with atmospheric CO_2 were too slow to be estimated.

XRD results indicated brucite was replaced by nesquehonite [$MgCO_3 \cdot 3H_2O$] (eq. 2) in all high pCO_2 reactors (SI Figure S6):

$$Mg(OH)_{2(s)} + HCO_3^-{}_{(aq)} + H^+_{(aq)} + H_2O_{(l)} \rightarrow MgCO_3 \cdot 3H_2O_{(s)} \qquad \text{(eq. 2)}$$

Nesquehonite was first detected within 8 h in 10% CO_2 1 and within 6 h in 10% CO_2 2 using carbon abundance analysis. It was detected within 2 h in the 50% and 100% CO_2 experiments. Minor amounts of phases that were not identifiable by XRD were formed in all high pCO_2 reactors and the atmospheric CO_2 experiment (SI Figure S6-S7). In the atmospheric CO_2 experiment, carbon abundance in the solids increased by 2.6%, identifying this phase as a carbonate. The unidentified phase was replaced by dypingite [$Mg_5(CO_3)_4(OH)_2 \cdot 5H_2O$] as the reaction progressed in 10% 1 and 2. XRD and %C data indicated carbonation was completed within 102 h in the 10% CO_2 reactors, by the 22 h and 12 h sampling points in 50% CO_2 1 and 2, respectively, and between 6 and 10 h in both 100% CO_2 reactors (SI Figure S6). Reaction end points between these times were inferred by the final decline in pH indicative of brucite removal.

As observed by SEM, precipitates from the 10% and 50% CO_2 experiments included elongate crystals consistent with the morphology of nesquehonite,[27] along with

flaky, poorly crystalline material and pseudo-rosettes (SI Figure S8). This morphology is typical of dypingite,[19,54] and is likely representative of both dypingite and the unidentified carbonate phase in the high pCO_2 experiments. Precipitates from the 100% CO_2 experiments were dominated by nesquehonite crystals (SI Figure S8).

Other experimental studies have used elevated CO_2 concentrations to precipitate nesquehonite by replacement of brucite or carbonation of $MgCl_2$ in solution,[27,31,55,56] which is consistent with this study. With a Mg:C ratio of 1:1, nesquehonite optimizes the amount of carbon stored per cation, an advantage for sequestration purposes. Dypingite and the unidentified carbonate phase may be reaction intermediates[57] or products of nesquehonite dehydration[58] between sampling and analysis, as depicted in SEM images, wherein flaky material armors nesquehonite crystals (SI Figure S8).

Initial %C values of solids ranged from 0.76-1.10% owing to the presence of primary dolomite [$CaMg(CO_3)_2$]. Carbon abundance in solid samples increased with time in each high pCO_2 experiment, followed by stabilization between 7.85 and 8.29% within 100, ~12, and 10 h in the 10%, 50%, and 100% CO_2 experiments, respectively (SI Figure S5). This is consistent with formation of nesquehonite, which ideally contains 8.68% carbon. Carbon abundance increased to 3.6% after 2856 h in the atmospheric CO_2 experiment. The mass of CO_2 sequestered in the high pCO_2 experiments was calculated using %C data assuming that dolomite mass remained constant and that CO_2 was stored primarily within nesquehonite. A total of 317 g of nesquehonite (~101 g CO_2) and 253 g (~81 g CO_2) were formed in 10% CO_2 1 and 2, respectively. In 50% CO_2 1 and 2, 275 g of nesquehonite (~88 g CO_2) and 244 g of nesquehonite (~78 g CO_2) were formed, respectively. A total mass of 223 g of nesquehonite (~71 g CO_2) and 254 g of

nesquehonite (~81 g CO_2) was precipitated in 100% CO_2 1 and 2, respectively. Discrepancies between duplicate reactors are attributed to imperfect mixing causing minor amounts of brucite to remain uncarbonated. The mass of carbon mineralized in the atmospheric CO_2 experiment was calculated using %C data assuming that brucite mass remained relatively unchanged, which is justified by the relative peak heights in the XRD data. A total of ~14 g CO_2 was captured over 2856 h.

Carbonation rates in the high pCO_2 experiments were calculated as follows (eq. 3):

$$CO_2 \text{ sequestration rate (g } CO_2\text{/g brucite/h)} = [(m_{fnsq} / M_{nsq}) \times M_{CO_2}] / (m_{ibrc} \times t_h) \quad \text{(eq. 3)}$$

Where m_{fnsq} is the final mass of nesquehonite (g), m_{ibrc} is the initial brucite mass (g), t_h is the time of reaction completion (h), and M_{nsq} and M_{CO_2} are the molar masses of nesquehonite and CO_2 (g/mol), respectively. In the atmospheric CO_2 experiment, the carbonation rate was calculated based on the rate of increase of %C in the solids. The rates of CO_2 sequestration using laboratory air, and average rates between duplicate 10%, 50%, and 100% CO_2 experiments were ~3.30×10^{-5}, 7.78×10^{-3}, 4.26×10^{-2}, and 8.00×10^{-2} g CO_2/g brucite/h, respectively. Dissolution and carbonation rates and CO_2 mass balances are summarized in Table 1.

Reaction mechanism. Brucite dissolution is a surface controlled reaction[39,41,59] that is accelerated with increased acidity and concentration of certain organic and inorganic ligands, such as HCO_3^-.[39,41,60] Proton and ligand promoted dissolution occur in

parallel; their effect is additive.[60] Ligands that promote brucite dissolution are those that form protonated ions at neutral to weakly alkaline pH (e.g., HCO_3^-), whereas those that are deprotonated inhibit dissolution (e.g., CO_3^{2-}).[39,60] Therefore, aqueous carbonate species may enhance or inhibit brucite dissolution depending on the solution pH. Previous studies have documented a dependence of brucite and MgO dissolution rate on HCO_3^- concentration.[31,60] As HCO_3^- is the dominant aqueous carbonate species in the experimental pH range,[61] dissolution and hydration of CO_2 may accelerate brucite dissolution via the direct effect of increasing HCO_3^- concentration and the indirect effect of increasing acidity. These effects cannot be separated in the high pCO_2 experiments, as neither pH nor DIC were fixed. Increased DIC concentration should also promote brucite carbonation by facilitating carbonate precipitation at lower Mg concentration, as suggested by Chen et al.[62] to account for enhanced carbonation of olivine in $NaHCO_3$ solutions.

To discern the effect of elevated pCO_2 on brucite carbonation rate, experimental conditions were modeled using PHREEQC.[48] Experimentally determined, steady-state, far from equilibrium rate laws dependent on pH[41] and ligand (HCO_3^-) concentration[60] were used, and are provided in the SI. Nesquehonite precipitation and CO_2 uptake were simulated as equilibrium processes. Modeling revealed that experimental dissolution and carbonation rates exceeded those predicted with proton promoted dissolution and high DIC promoted carbonate precipitation alone. With 100% CO_2, the experimental carbonation rate is 6-fold faster than predicted due to acidity promoted dissolution (Figure 4). Comparison of experimental dissolution rates with the pH-dependent rate law of Pokrovsky and Schott[41] highlights the discrepancy between the experimental rates and

those predicted due to proton promoted dissolution (SI Figure S9). In this study, dissolution rate is calculated based on the time to dissolve brucite of a specified mass, rather than an instantaneous rate based on the flux of Mg^{2+}; this could in part explain the divergence from the Pokrovsky and Schott rate law,[41] as the instantaneous rate was likely not constant. Experimental carbonation rates fell between those predicted by pH and HCO_3^- promoted dissolution (Figure 4), implying that HCO_3^- promoted brucite dissolution is likely an important mechanism enhancing brucite carbonation, yet the CO_2 supply was insufficient to achieve the maximum predicted rates.

Rate limitation. The fractionation of carbon stable isotopes can be used to infer the relative rates of processes that involve CO_2 and thus help identify rate limitations.[30] All isotopic data are reported in δ-notation relative to Vienna Pee Dee Belemnite (VPDB) in units of per mil (‰). The $\delta^{13}C_{CO_{2(g)}}$ values of the gas supply for the 10%, 50%, and 100% CO_2 experiments were -35‰, -37‰, and -32‰, respectively. Differences in initial $\delta^{13}C_{CO_{2(g)}}$ values are due to the use of different CO_2 tanks for each experiment. Equilibrium fractionation between $CO_{2(g)}$ and HCO_3^- is +7.9‰ at 25°C,[63] therefore, the equilibrium $\delta^{13}C_{DIC}$ values for the high pCO_2 experiments should be between ~-24‰, to -29‰. Divergence from the equilibrium $\delta^{13}C_{DIC}$ value increased in the first 36 h in 10% CO_2 1 and 2, before rising to reach equilibrium composition after ~175 h (Figure 5A). Wilson et al. observed a similar negative trend in $\delta^{13}C_{DIC}$ values during carbonation of a $MgCl_2$ solution using atmospheric CO_2, which was attributed to a kinetic isotope fractionation effect due to slow uptake of $CO_{2(g)}$ into solution.[30] In the 50% and 100% CO_2 experiments, equilibrium $^{13}C_{DIC}$ composition was obtained after 56 and 43 h,

respectively (Figure 5A). Yet, mineralogical data indicated carbonation was complete within 75, 12, and 7 h in the 10%, 50% and 100% CO_2 experiments, respectively. This implies that isotopic equilibrium between CO_2 in the gas and aqueous phase was not achieved during the carbonation reaction, but is only approached when the DIC sink, carbonate mineral precipitation, is ceased.

Due to the presence of dolomite in the initial material, early time $\delta^{13}C$ values of solids are not representative of precipitated carbonate (~-4.4‰). A cut off of a minimum of 4% carbon in the solids (at least 80% of carbon in nesquehonite) was chosen to be representative of nesquehonite stable isotopic composition. Nevertheless, the presence of minor dolomite results in the solids being enriched relative to the precipitated nesquehonite. The $\delta^{13}C$ values of the solids (primarily nesquehonite) remained between -28.3‰ to -30.8‰, and -29.6‰ to -32.6‰ in 10% CO_2 1 and 2, respectively. A greater range in $\delta^{13}C$ values was recorded in the 50% CO_2 experiment, with values between -29.6‰ to -37.4‰, and -31.2‰ to -36.1‰ in 50% CO_2 1 and 2, respectively. In 100% CO_2 1 and 2, $\delta^{13}C$ values were between -25.0‰ to -30.1‰, and -25.6‰ to -31.0‰, respectively. Fresh carbonate could not be sampled therefore $\delta^{13}C$ values are cumulative for carbonate formed throughout each experiment. Insufficient carbonate precipitation occurred in the atmospheric CO_2 experiment to determine the ^{13}C composition of the carbonate.

The equilibrium $\delta^{13}C$ fractionation factor between nesquehonite and HCO_3^- has not been determined. However, the observed fractionation is consistent with the equilibrium carbon isotopic fractionation factor estimated by Wilson et al. for dypingite and HCO_3^- (3.8 ± 1.3‰ at 25°C).[30] The $\delta^{13}C$ values of solids generally deviate between

0-5‰ from values predicted assuming isotopic equilibrium is maintained with the average $\delta^{13}C_{DIC}$ value during carbonation (Figure 5B). The majority of $\delta^{13}C$ values of solids fall within the range of equilibrium composition estimated with the observed range of $\delta^{13}C_{DIC}$ values during carbonation (shaded area in Figure 5B). This suggests that nesquehonite precipitated approximately at isotopic equilibrium with DIC throughout carbonation. Moreover, nesquehonite saturation indices calculated using PHREEQC[48] indicate nesquehonite precipitated near chemical equilibrium (SI Figure S10). This implies carbonate mineral precipitation is not rate limiting for carbonation, rather the slow approach to isotopic equilibrium between $CO_{2(g)}$ and DIC indicates uptake of CO_2 is the limiting step for brucite carbonation.

During carbonation, DIC concentrations in experiments were consistently below $CO_{2(g)}$↔DIC equilibrium levels as predicted by PHREEQC[48] modeling (Figure 3A). This further indicates equilibrium between CO_2 in the gas and aqueous phase was not obtained during carbonation. Experimental carbonation rates were generally lower than predicted by modeling due to HCO_3^- promoted dissolution, with divergence increasing at lower pCO_2 (Figure 4). This is consistent with a kinetic limitation to uptake of CO_2 into solution, as equilibrium DIC concentrations were not achieved in the experiments, and divergence from $CO_{2(g)}$↔DIC equilibrium was greatest at lower pCO_2. This is in agreement with the stable isotopic data, indicating that uptake of CO_2 into solution is rate limiting for brucite carbonation even at elevated pCO_2. The implication is that if $CO_{2(g)}$↔DIC equilibrium could be attained, the brucite carbonation rate would be further accelerated. CO_2 uptake into solution is divided into two steps: (1) $CO_{2(g)}$ dissolution and (2) $CO_{2(aq)}$ hydration. $CO_{2(g)}$ dissolution involves the phase transfer from gaseous to

aqueous CO_2, whereas $CO_{2(aq)}$ hydration is the subsequent formation of H_2CO_3 or HCO_3^- depending on solution pH, which dissociate to form CO_3^{2-}.[64] It is well understood that dissociation is rapid, whereas the hydration of $CO_{2(aq)}$ is relatively slow.[64-66] An option for further enhancing CO_2 uptake into solution is to accelerate CO_2 hydration, which may be achieved through use of biological catalysts such as the carbonic anhydrase enzyme.[67-69]

Implications for carbon sequestration in mine tailings. Experimental data show a linear increase in brucite carbonation rate with pCO_2, resulting in a ~2400-fold acceleration with an increase from atmospheric pCO_2 (~0.04% CO_2) to 100% CO_2. Conversely, modeling using PHREEQC[48] reveals a non-linear relationship between carbonation rate and pCO_2 with both proton and HCO_3^- promoted dissolution (Figure 4). This implies that use of 100% CO_2 may not be necessary to achieve maximum carbonation rates if CO_2 uptake into solution were enhanced (Figure 4). Direct use of flue gas (e.g., ~17% CO_2)[70] from mine site power plants could be sufficient to achieve similar carbonation rates as use of purified CO_2. This is highly advantageous as it eliminates the cost of purifying CO_2.

Despite a kinetic limitation for uptake of CO_2 into solution, brucite carbonation rates achieved in experiments exceed that required to carbonate all the brucite produced annually at MKM. MKM produces ~0.11-0.28 Mt of brucite in tailings annually, and emits 370 kt/year of CO_2 equivalent GHGs.[37,44] Carbonation of brucite produced annually would offset mine emissions by ~22-57% (Figure 6), which is up to 4-fold faster than estimated passive carbonation rates.[37] A tax on carbon emissions implemented in July

2012 in Australia implies tailings carbonation may offer a significant financial benefit for Australian mines such as MKM (e.g., up to $4.8 million saved annually).[71] Complete carbonation of brucite accumulated in tailings stockpiles at MKM would sequester a total of 1-3 Mt of CO_2. This is a comparable sequestration rate to what is currently achieved at the largest geologic carbon sequestration demonstration projects (~1-2.8 Mt CO_2/year).[72,73]

Brucite is present in ultramafic tailings from other deposit types, such as chrysotile. In Québec, Canada, there are approximately 2 Gt of chrysotile mining residues.[43] At the Black Lake mine in Quebec, chrysotile milling residues contain ~1.8 wt.% brucite.[22] If these brucite contents are representative for the entire stockpile, up to 27 Mt of CO_2 could be sequestered via brucite carbonation alone.

Brucite carbonation represents only a small proportion of the total sequestration potential of ultramafic tailings, which consist primarily of Mg-silicate minerals. At MKM, accelerated carbonation of Mg-silicate minerals has the potential to sequester much more CO_2 than is emitted annually (Figure 6). Accelerated dissolution of silicate tailings minerals such as serpentine [$Mg_3Si_2O_5(OH)_4$] and forsterite [Mg_2SiO_4] is predicted with increased pCO_2 owing to proton promoted dissolution.[40,74] The effect of inorganic carbon ligands on silicate mineral dissolution is less certain (c.f., forsterite,[75] wollastonite,[75] and anorthite[76]), and the effect on serpentine dissolution is not well understood under conditions prevalent in mine tailings. The presence of ligands such as citrate have been found to enhance serpentine dissolution by several orders of magnitude over that predicted by pH promoted dissolution, and can be significant in pH ranges appropriate for carbonate precipitation.[51] If serpentine dissolution were similarly affected as brucite by

surface reactions involving the HCO_3^- ligand, total carbonation rates in tailings may be underestimated based on pH effects alone.

Acknowledgements

This research was funded by the Carbon Management Canada National Centre of Excellence and a Natural Sciences and Engineering Research Council of Canada (NSERC) Discovery Grant to GMD. Research by IMP was funded by an NSERC Postdoctoral Fellowship. We thank Viorel Atudorei, Timothy Mah, and Maureen Soon for analytical assistance. We appreciate the advice of Uli Mayer regarding geochemical modeling, and Shaun Barker regarding stable isotope analyses. We also thank the editors and three anonymous reviewers for their insightful comments that greatly improved this manuscript. This is publication 306 of the Mineral Deposit Research Unit.

Supporting Information Available

A detailed description of the experimental setup, analytical techniques, and additional results can be found in the Supporting Information. This information is available free of charge via the Internet at http://pubs.acs.org.

Literature Cited

(1) IPCC. *IPCC Climate Change 2007: Synthesis Report, An Assessment of the Intergovernmental Panel on Climate Change*; 2007; http://www.ipcc.ch/pdf/assessment-report/ar4/syr/ar4_syr.pdf.

(2) Hoffert, M. I.; Caldeira, K.; Benford, G.; Criswell, D. R.; Herzog, H.; Jain, A. K.; Kheshgi, H. S.; Lackner, K. S.; Lewis, J. S.; Lightfoot, D.; Manheimer, W.; Mankins, J. C.; Mauel, M. E.; Perkins, L. J.; Schlesinger, M. E.; Volk, T.; Wigley, T. M. L. Advanced technology paths to global climate stability: Energy for a greenhouse planet. *Science* **2002**, *298*, 981–897.

(3) Pacala, S.; Socolow, R. Stabilization wedges: Solving the climate problem for the next 50 years with current technologies. *Science* **2004**, *305*, 968–972.

(4) Broecker, W. S. CO_2 arithmetic. *Science* **2007**, *315*, 1371.

(5) Lackner, K. S. A guide to CO_2 sequestration. *Science* **2003**, *300*, 1677–1678.

(6) Seifritz, W. CO_2 disposal by means of silicates. *Nature* **1990**, *345*, 486.

(7) Lackner, K. S.; Wendt, C. H.; Butt, D. P.; Joyce, E. L.; Sharp, D. H. Carbon dioxide disposal in carbonate minerals. *Energy* **1995**, *20*, 1153–1170.

(8) Lackner, K. S.; Butt, D. P.; Wendt, C. H. Progress on binding CO_2 in mineral substrates. *Energy Convers. Manage.* **1997**, *38*, S259–S264.

(9) Sipilä, J.; Teir, S.; Zevenhoven, R. *Carbon dioxide sequestration by mineral carbonation: Literature review update 2005-2007*; Report 2008-1; Åbo Akademi University Heat Engineering Laboratory, 2008.

(10) Béarat, H.; Mckelvy, M. J.; Chizmeshya, A. V. G.; Sharma, R.; Carpenter, R. W. Magnesium hydroxide dehydroxylation/carbonation reaction processes: Implications for carbon dioxide mineral sequestration. *J. Am. Ceram. Soc.* **2002**, *85*, 742–748.

(11) Zevenhoven, R.; Teir, S.; Eloneva, S. Heat optimisation of a staged gas–solid mineral carbonation process for long-term CO_2 storage. *Energy* **2008**, *33*, 362–370.

(12) Gerdemann, S. J.; O'Connor, W. K.; Dahlin, D. C.; Penner, L. R.; Rush, H. Ex situ aqueous mineral carbonation. *Environ. Sci. Technol.* **2007**, *41*, 2587–2593.

(13) Fagerlund, J.; Teir, S.; Nduagu, E.; Zevenhoven, R. Carbonation of magnesium silicate mineral using a pressurised gas/solid process. *Energy Procedia* **2009**, *1*, 4907–4914.

(14) Krevor, S. C.; Lackner, K. S. Enhancing process kinetics for mineral carbon sequestration. *Energy Procedia* **2009**, *1*, 4867–4871.

(15) Koukouzas, N.; Gemeni, V.; Ziock, H. J. Sequestration of CO_2 in magnesium silicates, in Western Macedonia, Greece. *Int. J. Miner. Process.* **2009**, *93*, 179-186.

(16) Manning, D. A. C. Biological enhancement of soil carbonate precipitation: Passive removal of atmospheric CO_2 *Mineral. Mag.* **2008**, *72*, 639–649.

(17) Renforth, P.; Manning, D. A. C.; Lopez-Capel, E. Carbonate precipitation in artificial soils as a sink for atmospheric carbon dioxide. *Appl. Geochem.* **2009**, *24*, 1757–1764.

(18) Wilson, S. A.; Dipple, G. M.; Power, I. M.; Thom, J. M.; Anderson, R. G.; Raudsepp, M.; Gabites, J. E.; Southam, G. Carbon dioxide fixation within mine wastes of ultramafic-hosted ore deposits: Examples from the Clinton Creek and Cassiar chrysotile deposits, Canada. *Econ. Geol.* **2009**, *104*, 95–112.

(19) Power, I. M.; Wilson, S. A.; Thom, J. M.; Dipple, G. M.; Gabites, J. E.; Southam, G. The hydromagnesite playas of Atlin, British Columbia, Canada: A biogeochemical model for CO_2 sequestration. *Chem. Geol.* **2009**, *260*, 286–300.

(20) Schuiling, R. D.; Boer, P. L. D. Coastal spreading of olivine to control atmospheric CO_2 concentrations: A critical analysis of viability. Comment: Nature and laboratory models are different. *Int. J. Greenhouse Gas Control* **2010**, *4*, 855–856.

(21) Wilson, S. A.; Dipple, G. M.; Power, I. M.; Barker, S. L. L.; Fallon, S. J.; Southam, G. Subarctic weathering of mineral wastes provides a sink for atmospheric CO_2. *Environ. Sci. Technol.* **2011**, *45*, 7727–7736.

(22) Pronost, J.; Beaudoin, G.; Tremblay, J.; Constantin, M. Carbon sequestration kinetic and storage capacity of ultramafic mining waste. *Environ. Sci. Technol.* **2011**, 9413–9420.

(23) Huijgen, W. J. J.; Comans, R. N. J. Carbonation of steel slag for CO_2 sequestration: Leaching of products and reaction mechanisms. *Environ. Sci. Technol.* **2006**, *40*, 2790–2796.

(24) Wilson, S. A.; Raudsepp, M.; Dipple, G. M. Verifying and quantifying carbon fixation in minerals from serpentine-rich mine tailings using the Rietveld method with X-ray powder diffraction data. *Am. Mineral.* **2006**, *91*, 1331–1341.

(25) Dilmore, R.; Lu, P.; Allen, D.; Soong, Y.; Hedges, S.; Fu, J. K.; Dobbs, C. L.; Degalbo, A.; Zhu, C. Sequestration of CO_2 in mixtures of bauxite residue and saline wastewater. *Energy & Fuels* **2008**, *22*, 343–353.

(26) Eloneva, S.; Teir, S.; Salminen, J.; Fogelholm, C.-J.; Zevenhoven, R. Fixation of CO_2 by carbonating calcium derived from blast furnace slag. *Energy* **2008**, *33*, 1461–1467.

(27) Ferrini, V.; De Vito, C.; Mignardi, S. Synthesis of nesquehonite by reaction of gaseous CO_2 with Mg chloride solution: Its potential role in the sequestration of carbon dioxide. *J. Hazard. Mater.* **2009**, *168*, 832–837.

(28) Power, I. M.; Dipple, G. M.; Southam, G. Bioleaching of ultramafic tailings by *Acidithiobacillus* spp. for CO_2 sequestration. *Environ. Sci. Technol.* **2010**, *44*, 456–462.

(29) Gunning, P. J.; Hills, C. D.; Carey, P. J. Accelerated carbonation treatment of industrial wastes. *Waste Manage.* **2010**, *30*, 1081–1090.

(30) Wilson, S. A.; Barker, S. L. L.; Dipple, G. M.; Atudorei, V. Isotopic disequilibrium during uptake of atmospheric CO_2 into mine process waters: Implications for CO_2 sequestration. *Environ. Sci. Technol.* **2010**, *44*, 9522–9529.

(31) Back, M.; Bauer, M.; Stanjek, H.; Peiffer, S. Sequestration of CO_2 after reaction with alkaline earth metal oxides CaO and MgO. *Appl. Geochem.* **2011**, *26*, 1097–1107.

(32) Power, I. M.; Wilson, S. A.; Small, D. P.; Dipple, G. M.; Wan, W.; Southam, G. Microbially mediated mineral carbonation: Roles of phototrophy and heterotrophy. *Environ. Sci. Technol.* **2011**, *45*, 9061–9068.

(33) Bobicki, E. R.; Liu, Q.; Xu, Z.; Zeng, H. Carbon capture and storage using alkaline industrial wastes. *Prog. Energy Combust. Sci.* **2012**, *38*, 302-320.

(34) Mignardi, S.; De Vito, C.; Ferrini, V.; Martin, R. F. The efficiency of CO_2 sequestration via carbonate mineralization with simulated wastewaters of high salinity. *J. Hazard. Mater.* **2011**, *191*, 49-55.

(35) Morales-Flórez, V.; Santos, A.; Lemus, A.; Esquivias, L. Artificial weathering pools of calcium-rich industrial waste for CO_2 sequestration. *Chem. Eng. J.* **2011**, *166*, 132-137.

(36) Pronost, J.; Beaudoin, G.; Lemieux, J.-M.; Hébert, R.; Constantin, M.; Marcouiller, S.; Klein, M.; Duchesne, J.; Molson, J. W.; Larachi, F.; Maldague, X. CO_2-depleted warm air venting from chrysotile milling waste (Thetford Mines,

Canada): Evidence for in-situ carbon capture from the atmosphere. *Geology* **2012**, *40*, 275-278.

(37) Wilson, S. A. Mineral traps for greenhouse gases in mine tailings: A protocol for verifying and quantifying CO_2 sequestration in ultramafic mines. Ph.D. Dissertation, The University of British Columbia, Vancouver, BC, 2009.

(38) Bea, S. A.; Wilson, S. A.; Mayer, K. U.; Dipple, G. M.; Power, I. M.; Gamazo, P. Reactive transport modeling of natural carbon sequestration in ultramafic mine tailings. *Vadose Zone J.* **2012**, *11*, doi: 10.2136/vzj20110089

(39) Vermilyea, D. A. The dissolution of MgO and $Mg(OH)_2$ in aqueous solutions. *J. Electrochem. Soc.* **1969**, *116*, 1179–1183.

(40) Pokrovsky, O. S.; Schott, J. Kinetics and mechanism of forsterite dissolution at 25°C and pH from 1 to 12. *Geochim. Cosmochim. Acta* **2000**, *64*, 3313–3325.

(41) Pokrovsky, O.; Schott, J. Experimental study of brucite dissolution and precipitation in aqueous solutions: Surface speciation and chemical affinity control. *Geochim. Cosmochim. Acta* **2004**, *68*, 31–45.

(42) Chrysochoou, M.; Fakra, S. C.; Marcus, M. A.; Moon, D. H.; Dermatas, D. Microstructural analyses of Cr(VI) speciation in chromite ore processing residue (COPR). *Environ. Sci. Technol.* **2009**, *43*, 5461-5466.

(43) Larachi, F.; Daldoul, I.; Beaudoin, G. Fixation of CO_2 by chrysotile in low-pressure dry and moist carbonation: Ex-situ and in-situ characterizations. *Geochim. Cosmochim. Acta* **2010**, *74*, 3051-3075.

(44) BHP Billiton. Mt Keith Nickel Operations: Environmental Data. BHP Billiton Sustainability Reports, BHP Billiton, 2005; http://hsecreport.bhpbillton.com/wmc/2004/performance/mko/data

(45) Stolberg, D. J. S. Rehabilitation studies on tailings storage facilities in an arid hypersaline region, Ph.D. Dissertation, The University of Queensland, Brisbane, Australia, 2005.

(46) Barker, S. L. L.; Dipple, G. M.; Dong, F.; Baer, D. S. Use of laser spectroscopy to measure the $^{13}C/^{12}C$ and $^{18}O/^{16}O$ compositions of carbonate minerals. *Anal. Chem.* **2011**, *83*, 2220–2226.

(47) Craig, H. Isotopic standards for carbon and oxygen and correction factors for mass-spectrometric analysis of carbon dioxide. *Geochim. Cosmochim. Acta* **1957**, *12*, 133–149.

(48) Parkhurst, D. L.; Appelo, C. A. J. *User's Guide to PHREEQC (Version 2)— A Computer Program for Speciation, and Inverse Geochemical Calculations*; U.S. Geological Survey Water-Resources Investigations Report 99-4259; 1999.

(49) Teir, S.; Kuusik, R.; Fogelholm, C.; Zevenhoven, R. Production of magnesium carbonates from serpentinite for long-term storage of CO_2. *Int. J. Miner. Process.* **2007**, *85*, 1–15.

(50) Eloneva, S.; Teir, S.; Salminen, J. Fogelholm,; C.-J.; Zevenhoven, R. Steel converter slag as a raw material for precipitation of pure calcium carbonate. *Ind. Eng. Chem. Res.* **2008**, *47*, 7104–7111.

(51) Krevor, S. C. M.; Lackner, K. S. Enhancing serpentine dissolution kinetics for mineral carbon dioxide sequestration. *Int. J. Greenhouse Gas Control* **2011**, *5*, 1073-1080.

(52) Park, A.-Hyung A.; Fan, L.-Shih CO_2 mineral sequestration: Physically activated dissolution of serpentine and pH swing process. *Chem. Eng. Sci.* **2004**, *59*, 5241-5247.

(53) Konigsberger, E.; Konigsberger, L.-C.; Gamsjager, H. Low-temperature thermodynamic model for the system Na_2CO_3-$MgCO_3$-$CaCO_3$-H_2O. *Geochim. Cosmochim. Acta* **1999**, *63*, 3105–3119.

(54) Power, I. M.; Wilson, S. A.; Thom, J. M.; Dipple, G. M.; Southam, G. Biologically induced mineralization of dypingite by cyanobacteria from an alkaline wetland near Atlin, British Columbia, Canada. *Geochem. Trans.* **2007**, *8*, 13.

(55) Hanchen, M.; Prigiobbe, V.; Baciocchi, R.; Mazzotti, M. Precipitation in the Mg-carbonate system - effects of temperature and CO_2 pressure. *Chem. Eng. Sci.* **2008**, *63*, 1012–1028.

(56) Zhao, L.; Sang, L.; Chen, J.; Ji, J.; Teng, H. H. Aqueous carbonation of natural brucite: Relevance to CO_2 sequestration. *Environ. Sci. Technol.* **2010**, *44*, 406–411.

(57) Hopkinson, L.; Kristova, P.; Rutt, K.; Cressey, G. Phase transitions in the system MgO - CO_2 - H_2O during CO_2 degassing of Mg-bearing solutions. *Geochim. Cosmochim. Acta* **2011**, *76*, 1–13.

(58) Ballirano, P.; De Vito, C.; Ferrini, V.; Mignardi, S. The thermal behaviour and structural stability of nesquehonite, $MgCO_3 \cdot 3H_2O$, evaluated by in situ laboratory parallel-beam X-ray powder diffraction: New constraints on CO_2 sequestration within minerals. *J. Hazard. Mater.* **2010**, *178*, 522-528.

(59) Jordan, G. Dissolution rates and activation energy for dissolution of brucite (001): A new method based on the microtopography of crystal surfaces. *Geochim. Cosmochim. Acta* **1996**, *60*, 5055–5062.

(60) Pokrovsky, O. S.; Schott, J.; Castillo, A. Kinetics of brucite dissolution at 25°C in the presence of organic and inorganic ligands and divalent metals. *Geochim. Cosmochim. Acta* **2005**, *69*, 905–918.

(61) Langmuir, D. *Aqueous Environmental Geochemistry*; Prentice Hall: Upper Saddle River, USA, 1997.

(62) Chen, Z.-Y.; O'Connor, W. K.; Gerdemann, S. J. Chemistry of aqueous mineral carbonation for carbon sequestration and explanation of experimental results. *Environ. Prog.* **2006**, *25*, 161-166.

(63) Mook, W.; Bommerson, J.; Staverman, W. Carbon isotope fractionation between dissolved bicarbonate and gaseous carbon dioxide. *Earth Planet. Sci. Letters* **1974**, *22*, 169–176.

(64) Stumm, W.; Morgan, J. J. *Aquatic chemistry*; Schnoor, J. L.; Zehnder, A., Eds. 3rd ed.; John Wiley & Sons, Inc.: New York, NY, 1996.

(65) Lasaga, A. *Kinetic Theory in the Earth Sciences*; Princeton University Press: Princeton, USA, 1998.

(66) Sullivan, B. P.; Krist, K.; Guard, H. E. *Electrical and electorcatalytic reactions of carbon dioxide*; Elsevier: Amsterdam, NL, 1993.

(67) Mirjafari, P.; Asghari, K.; Mahinpey, N. Investigating the application of enzyme carbonic anhydrase for CO_2 sequestration purposes. *Ind. Eng. Chem. Res.* **2007**, *2*, 921–926.

(68) Sharma, A.; Bhattacharya, A. Enhanced biomimetic sequestration of CO_2 into $CaCO_3$ using purified carbonic anhydrase from indigenous bacterial strains. *J. Mol. Catal. B: Enzym.* **2010**, *67*, 122–128.

(69) Favre, N.; Christ, M. L.; Pierre, A. C. Biocatalytic capture of CO_2 with carbonic anhydrase and its transformation to solid carbonate. *J. Mol. Catal. B: Enzym.* **2009**, *60*, 163–170.

(70) Kikkinides, E. S.; Yang, R. T.; Cho, S. H. Concentration and recovery of CO_2 from flue gas by pressure swing adsorption. *Ind. Eng. Chem. Res.* **1993**, *32*, 2714–2720.

(71) Australian Government. Securing a clean energy future: The Australian government's climate change plan, 2011;

http://www.cleanenergyfuture.gov.au/wp-content/uploads/2011/07/Consolidated-Final.pdf.

(72) Whittaker, S.; Rostron, B.; Hawkes, C.; Gardner, C.; White, D.; Johnson, J. A decade of CO_2 injection into depleting oil fields: monitoring and research activities of the IEA GHG Weyburn-Midale CO_2 Monitoring and Storage Project. *Energy Procedia* **2011**, *4*, 6069–6076.

(73) Michael, K.; Allinson, G.; Golab, A.; Sharma, S.; Shulakova, V. CO_2 storage in saline aquifers II – experience from existing storage operations. *Energy Procedia* **2009**, *1*, 1973–1980.

(74) Bales, R. C.; Morgan, J. J. Dissolution kinetics of chrysotile at pH 7 to 10. *Geochim. Cosmochim. Acta* **1985**, *49*, 2281-2288.

(75) Golubev, S. V.; Pokrovsky, O. S.; Schott, J. Experimental determination of the effect of dissolved CO_2 on the dissolution kinetics of Mg and Ca silicates at 25 °C. *Chem. Geol.* **2005**, *217*, 227–238.

(76) Berg, A.; Banwart, S. A. Carbon dioxide mediated dissolution of Ca-feldspar: Implications for silicate weathering. *Chem. Geol.* **2000**, *163*, 25-42.

Figure Captions

Figure 1. Schematic of carbon mineralization *in situ* in a tailings storage facility.

Figure 2. Plots of pH (A) in high pCO_2 experiments versus time. Dashed lines are results from PHREEQC[48] models assuming kinetically controlled brucite dissolution and equilibrium $CO_{2(g)}$ dissolution. Dissolved inorganic carbon (DIC) (diamonds) and pH (+) in the long-term atmospheric CO_2 experiment, and DIC (triangles) and pH (circles) in controls versus time (B). The dashed line in (B) indicates the DIC concentration at equilibrium with atmospheric CO_2. Open symbols and solid symbols in (A) represent duplicates 1 and 2, respectively. Arrows above the graph in (A) represent the duration of the carbonation reaction in the 100%, 50% and 10% CO_2 experiments, respectively.

Figure 3. Plots of dissolved inorganic carbon concentration (DIC) (A), and Mg concentration (B) in high pCO_2 experiments versus time. Dashed lines are results from PHREEQC[48] models assuming kinetically controlled brucite dissolution and equilibrium $CO_{2(g)}$ dissolution. Open symbols and solid symbols represent duplicates 1 and 2, respectively. Arrows above the graphs represent the duration of the carbonation reaction in the 100%, 50% and 10% CO_2 experiments, respectively.

Figure 4. Experimentally determined and modeled (PHREEQC)[48] brucite carbonation rate versus pCO_2 in experiments using ligand (Pokrovksy et al.)[60] and pH (Pokrovsky and

Schott)[41] dependent brucite dissolution rate laws. Open symbols and solid symbols represent duplicates 1 and 2, respectively.

Figure 5. Deviation from calculated equilibrium $\delta^{13}C_{DIC}$ values relative to VPDB in high pCO_2 experiments versus time using the fractionation factor of Mook et al. (A).[63] Deviation from calculated equilibrium $\delta^{13}C$ values of solids with the average $\delta^{13}C_{DIC}$ during carbonation using the fractionation factor of Wilson et al.[30] in high pCO_2 experiments versus time of sampling (B). Shaded area represents the range of equilibrium $\delta^{13}C$ values of solids with the observed range in $\delta^{13}C_{DIC}$ values during carbonation. Open and solid symbols represent duplicates 1 and 2, respectively. Arrows above the graphs represent the duration of the carbonation reaction in the 100%, 50% and 10% CO_2 experiments, respectively.

Figure 6. Comparison of range of passive annual carbonation rates at Diavik Diamond Mine, Northwest Territories, Canada,[21] Clinton Creek Chrysotile mine, Yukon Territory, Canada,[18] and the Mount Keith Nickel Mine (MKM), Western Australia[37] with annual GHG emissions at various mine sites, total sequestration capacity, and potential annual carbonation rates at MKM via accelerated brucite carbonation.

Table 1. CO_2 mass balance and brucite dissolution and carbonation rates[‡]

***p*CO₂**	**Dissolution rate***	**Carbonation rate***	**$CO_{2(g)}$ supplied**	**CO_2 in aqueous phase**	**CO_2 in solid**	**Total CO_2 sequestered**	****Efficiency**
(% of 1 atm)	(mol brucite/h)	(mol CO_2 /h)	(g)	(g)	(g)	(g)	(%)
0.04	No data	1.1×10^{-4}	1768	8×10^{-2}	14	14	0.8%
10	0.03	0.03	223	6	91	97	43%
50	0.22	0.15	180	9	83	92	51%
100	0.36	0.27	211	16	76	92	44%

[‡]All values are averages for duplicate reactors.

*Dissolution and carbonation rates have been converted to mol/h for ease of comparison.

**Efficiency calculated as Mass CO_2 sequestered in solid ÷ Mass $CO_{2(g)}$ supplied during carbonation.

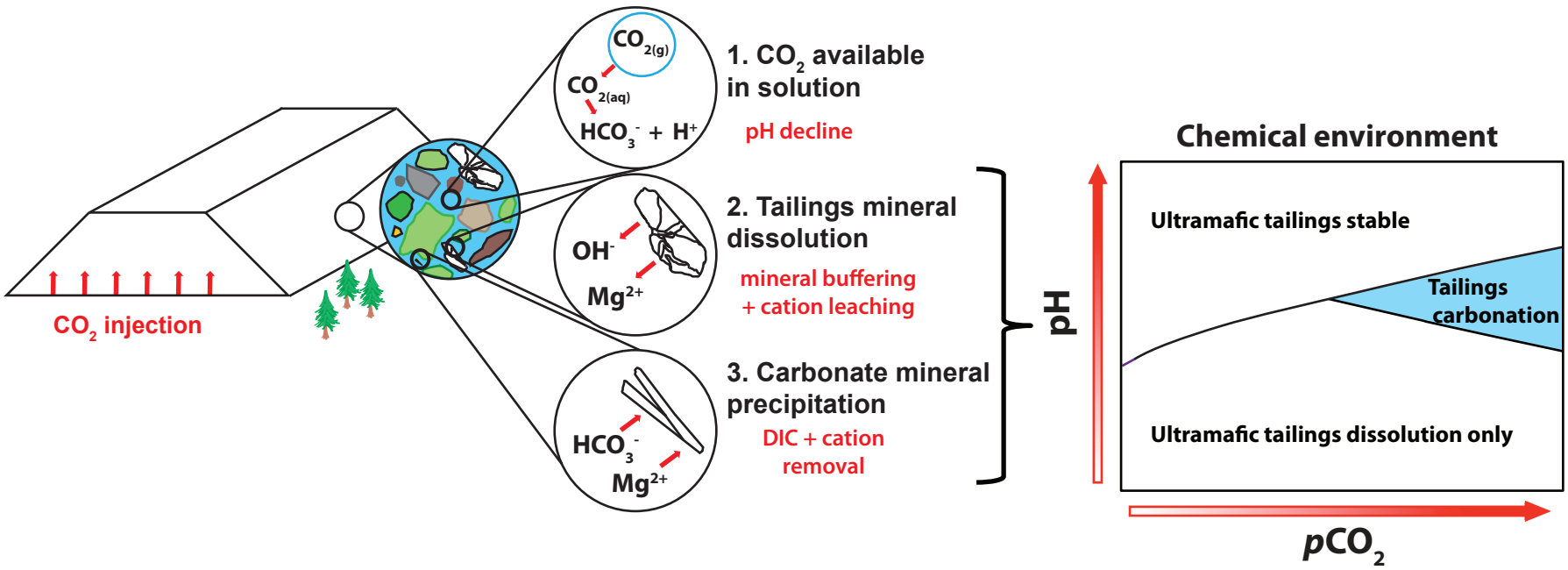
CO2(g)
CO2(aq)
HCO3- + H+
1. CO2 available in solution
pH decline
OH-
Mg2+
2. Tailings mineral dissolution
mineral buffering + cation leaching
HCO3-
Mg2+
3. Carbonate mineral precipitation
DIC + cation removal
CO2 injection
pH
Chemical environment
Ultramafic tailings stable
Tailings carbonation
Ultramafic tailings dissolution only
pCO2

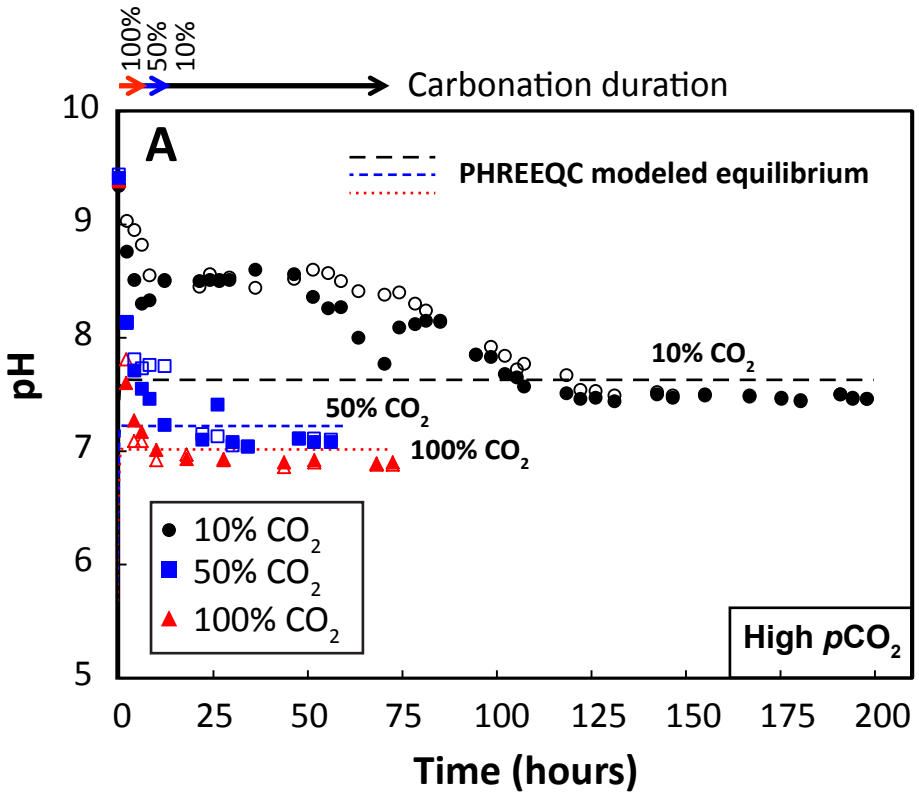
100%
50%
10%
Carbonation duration
A
PHREEQC modeled equilibrium
10% CO2
50% CO2
100% CO2
10% CO2
50% CO2
100% CO2
High pCO2
pH
Time (hours)

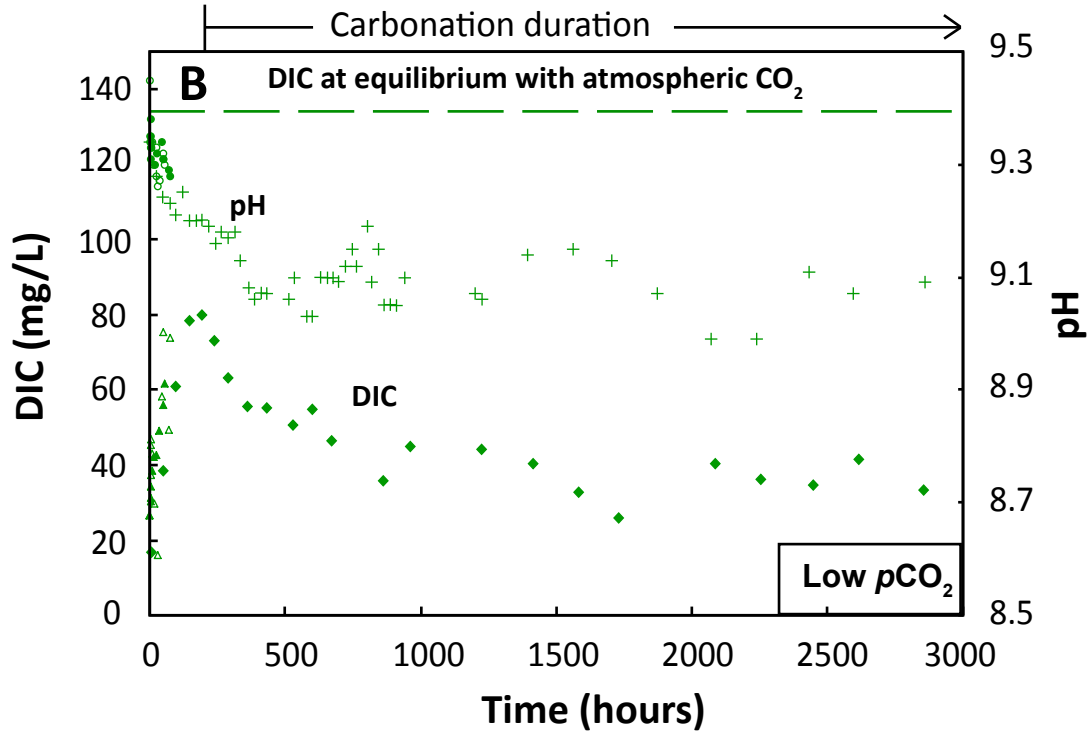
Carbonation duration
B
DIC at equilibrium with atmospheric CO2
pH
DIC
Low pCO2
DIC (mg/L)
pH
Time (hours)

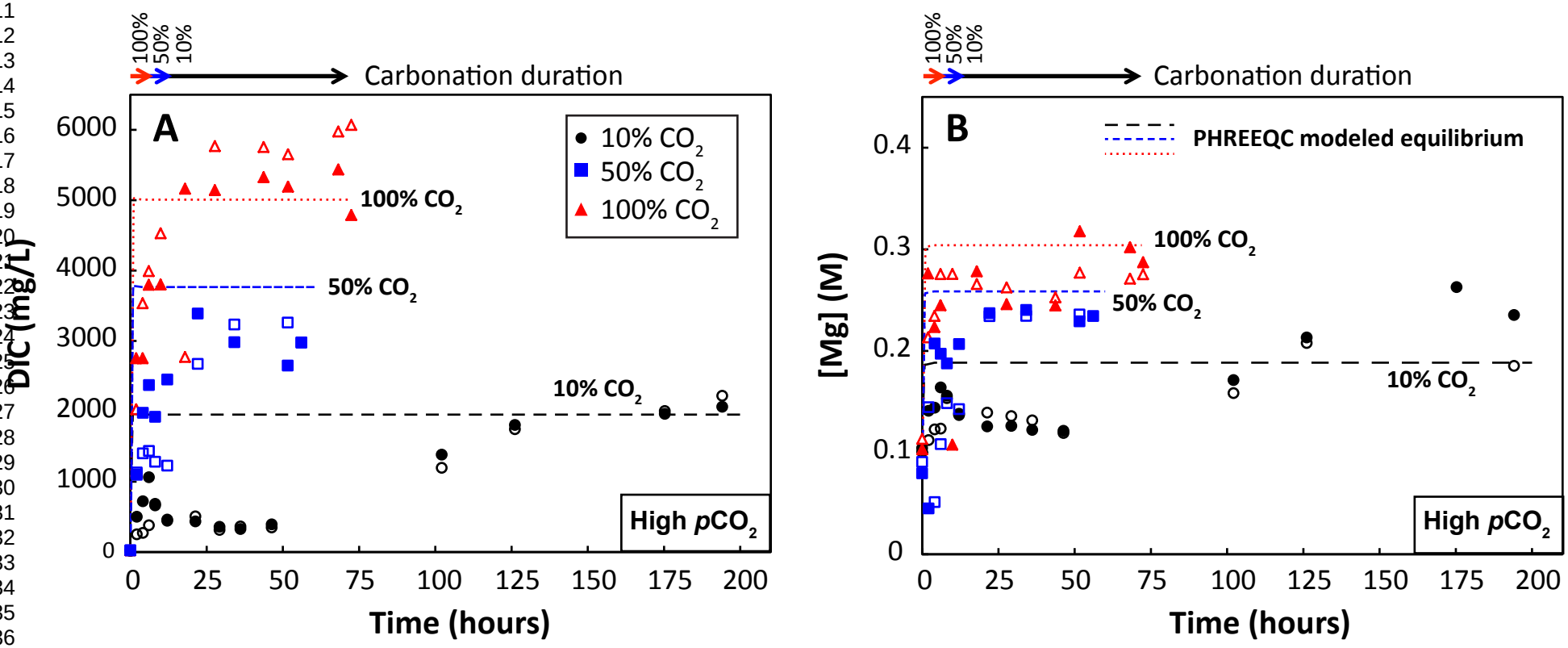
100%
50%
10%
Carbonation duration
A
10% CO2
50% CO2
100% CO2
100% CO2
50% CO2
10% CO2
High pCO2
DIC (mg/L)
Time (hours)
0
1000
2000
3000
4000
5000
6000
0
25
50
75
100
125
150
175
200

100%
50%
10%
Carbonation duration
B
PHREEQC modeled equilibrium
100% CO2
50% CO2
10% CO2
High pCO2
[Mg] (M)
Time (hours)
0
0.1
0.2
0.3
0.4
0
25
50
75
100
125
150
175
200

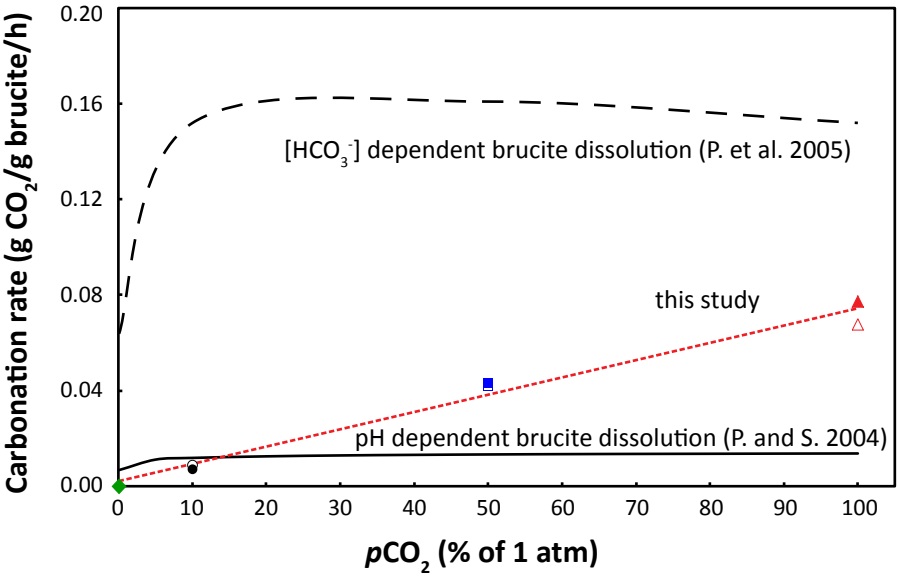
Carbonation rate (g CO2/g brucite/h)
0.20
0.16
0.12
0.08
0.04
0.00
0
10
20
30
40
50
60
70
80
90
100
pCO2 (% of 1 atm)
[HCO3-] dependent brucite dissolution (P. et al. 2005)
this study
pH dependent brucite dissolution (P. and S. 2004)

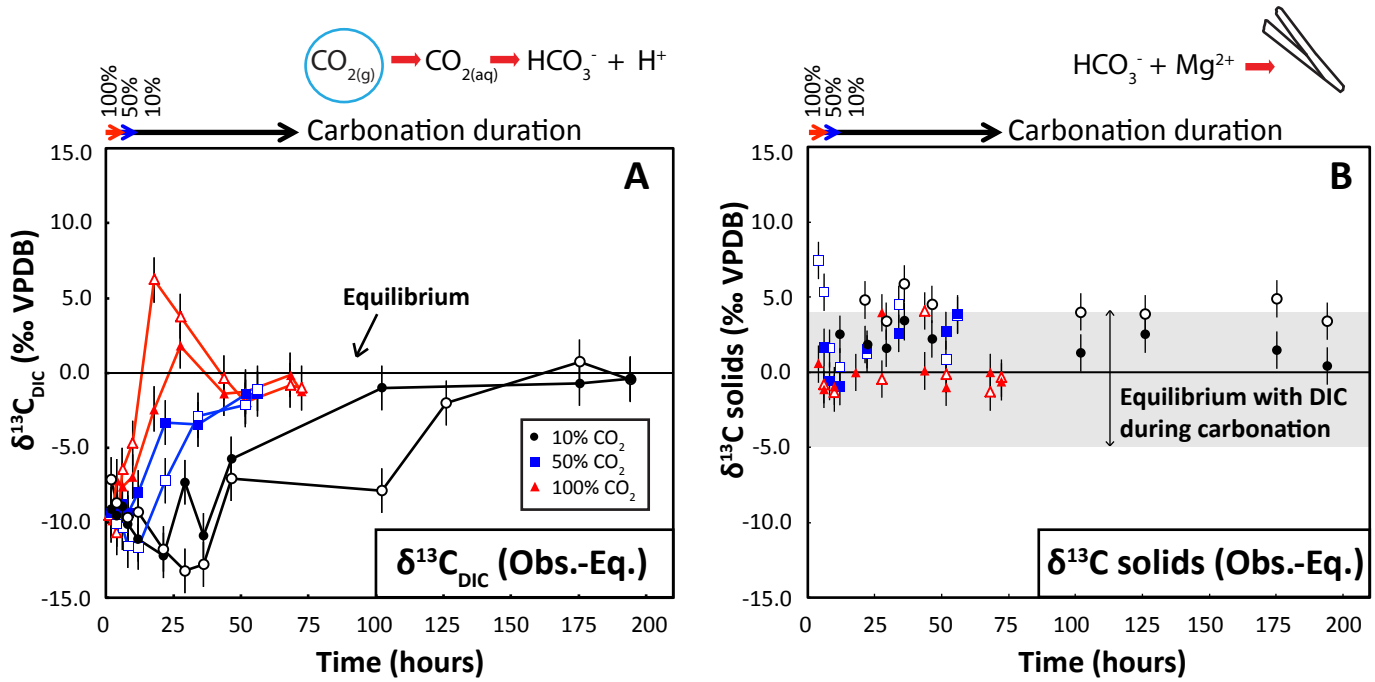
CO2(g)
CO2(aq)
HCO3- + H+
100%
50%
10%
Carbonation duration
A
Equilibrium
δ13CDIC (‰ VPDB)
10% CO2
50% CO2
100% CO2
δ13CDIC (Obs.-Eq.)
Time (hours)
HCO3- + Mg2+
B
δ13C solids (‰ VPDB)
Equilibrium with DIC
during carbonation
δ13C solids (Obs.-Eq.)

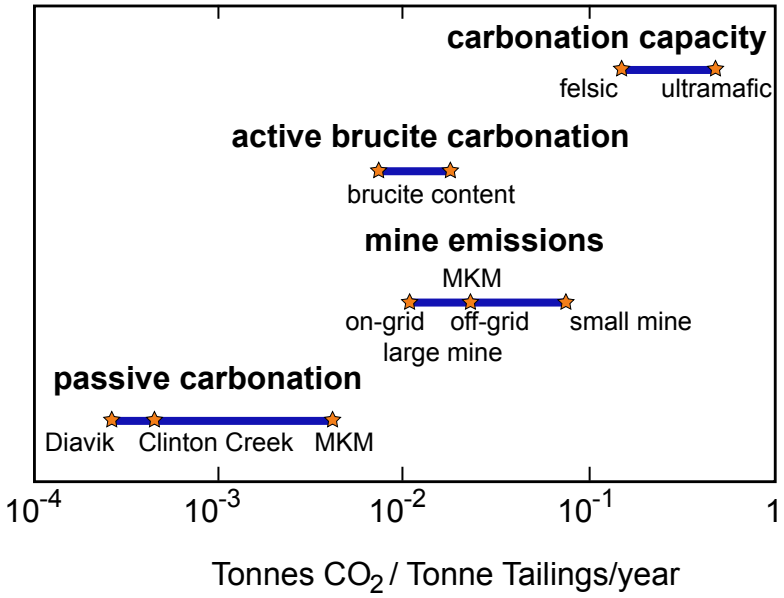
carbonation capacity
felsic
ultramafic
active brucite carbonation
brucite content
mine emissions
MKM
on-grid
off-grid
small mine
large mine
passive carbonation
Diavik
Clinton Creek
MKM
10-4
10-3
10-2
10-1
1
Tonnes CO2 / Tonne Tailings/year

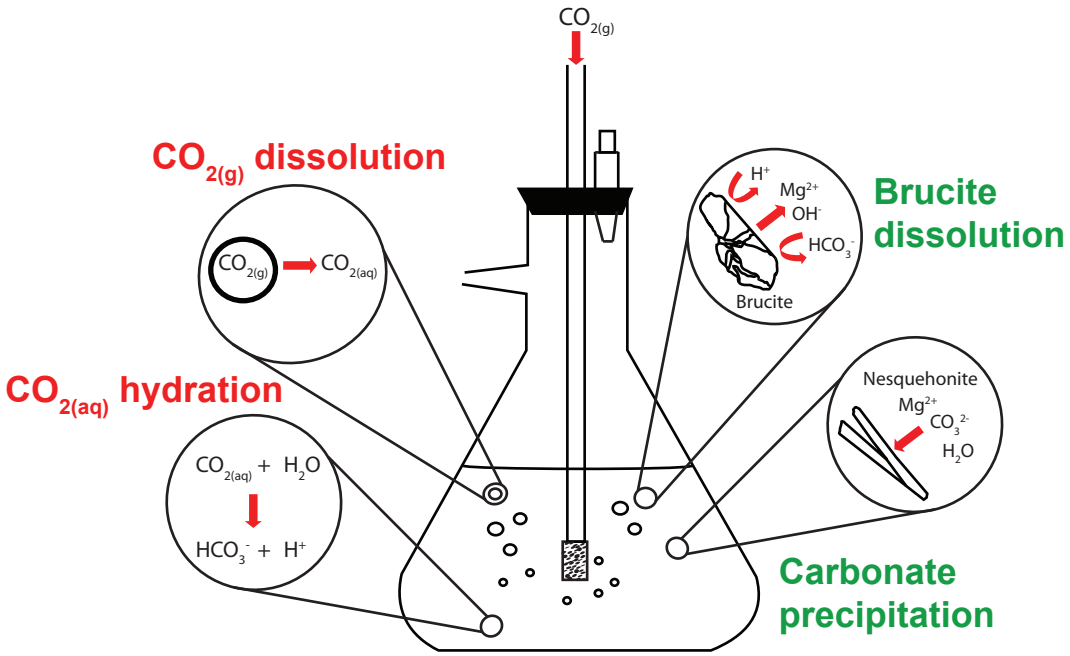
$CO_{2(g)}$
$CO_{2(g)}$ dissolution
$CO_{2(g)}$ → $CO_{2(aq)}$
$CO_{2(aq)}$ hydration
$CO_{2(aq)} + H_2O$
$HCO_3^- + H^+$
H^+
Mg^{2+}
OH^-
HCO_3^-
Brucite
Brucite dissolution
Nesquehonite
Mg^{2+}
CO_3^{2-}
H_2O
Carbonate precipitation